Title

Evaluation of computer-aided design software methods for assessment of the three-dimensional geometry of the canine radius.

Journal

American Journal of Veterinary Research, 82(6)

ISSN

0002-9645

Authors

Park, Karen M
Marcellin-Little, Denis J
Garcia, Tanya C

Publication Date

2021-06-01

DOI

10.2460/ajvr.82.6.435

Peer reviewed

Evaluation of computer-aided design software methods for assessment of the three-dimensional geometry of the canine radius

Karen M. Park DVM
Denis J. Marcellin-Little DEDV
Tanya C. Garcia MS

Received August 24, 2020.
Accepted October 29, 2020.

From the Veterinary Orthopedic Research Laboratory, School of Veterinary Medicine, University of California-Davis, Davis, CA 95616.

Address correspondence to Dr. Marcellin-Little (djmarcel@ucdavis.edu).

OBJECTIVE
To describe methods to measure the 3-D orientation of the proximal, diaphyseal, and distal segments of the canine radius by use of computer-aided design software (CADS) and to compare the repeatability and reliability of measurements derived by those methods.

SAMPLE
31 canine radii with biapical deformities and 24 clinically normal (control) canine radii.

PROCEDURES
Select CT scans of radii were imported into a CADS program. Cartesian coordinate systems for the humerus and proximal, diaphyseal, and distal radial segments were developed. The orientation of each radial segment in the frontal, sagittal, and transverse planes was measured in triplicate by 3 methods. The repeatability and reliability of those measurements were calculated and compared among the 3 measurement methods.

RESULTS
The mean ± SD within-subject repeatability of radial angular measurements for all 3 methods was 1.40 ± 0.67° in the frontal plane, 3.17 ± 2.21° in the sagittal plane, and 3.01 ± 1.11° in the transverse plane for control radii and 2.56 ± 1.95° in the frontal plane, 3.59 ± 2.39° in the sagittal plane, and 3.47 ± 1.19° in the transverse plane for abnormal radii. Mean ± SD bias between radial measurement methods was 1.88 ± 2.07° in the frontal plane, 6.44 ± 6.80° in the sagittal plane, and 2.27 ± 2.81° in the transverse plane.

CONCLUSIONS AND CLINICAL RELEVANCE
Results indicated that use of CADS to assess the 3-D orientation of the proximal, diaphyseal, and distal segments of normal and abnormal canine radii yielded highly repeatable and reliable measurements. (*Am J Vet Res* 2021;82:435–448)

Deformities of the radius are the most common bone deformities in dogs.[1] They generally result from premature closure of ulnar or radial physes, trauma, or genetically driven abnormal limb growth such as chondrodystrophy or chondrodysplasia. Radial deformities can be managed with surgical procedures such as corrective osteotomy and stabilization of the radius with a bone plate or external skeletal fixator.[1,2]

Clinically, measurements of bone geometry are most commonly made on orthogonal (craniocaudal and mediolateral) radiographic views.[3] Joint orientation, defined as the relative orientation of 2 adjacent bones within a single plane, is also often measured by use of radiographic views.[4,5] Those views are 2-D images and, unfortunately, may lack accuracy or repeatability because of x-ray beam divergence, differential magnification, suboptimal bone positioning, and the influence of a deformity in 1 plane on the measurement of a deformity in a perpendicular plane.[6,7] Evaluation of oblique radiographic views is recommended to compensate for that lack of accuracy.[6] Radiographic distortion and the challenge of obtaining accurate patient positioning for measurement of bone deformities have also been described.[8,9] The 3-D measurement of the geometry or orientation of a joint, bone, or bone segment may be warranted to enhance precision of corrective procedures. Cross-sectional images of deformed limbs can be acquired by use of CT. Multiplanar 2-D and 3-D reconstructions of CT images have been used to further assess the geometry of deformed bones.[1–3] Computer-aided design software has also been used to assess the geometry of normal and abnormal bones[10–13] and plan complex or-

ABBREVIATIONS

BFA	Best fit capture of the articular surface
BFC	Best fit elliptical cylinders
CADS	Computer-aided design software
CART	Classification and regression tree
CV	Coefficient of variation
DPC	Diaphyseal centerline
STG	Surface tangent
TLA	Three landmarks along the edge of the articular surface

thopedic procedures, such as total joint arthroplasty and limb-sparing surgeries.[14,15]

Several studies have described the accuracy of surgical correction for deformities of the radius,[16] femur,[17] tibia,[18] and mandible[19] following the use of 3-D imaging and CADS for preoperative planning. To acquire 3-D measurements with CADS, construction of Cartesian coordinate systems based on the anatomic features of the joints, bones, or bone segments under consideration is required. Evaluation of the orientation of a bone in space requires comparison of a local coordinate system (ie, the bone in question) with a global coordinate system.[20] Evaluation of the orientation of bones relative to each other within a joint requires comparison of the local coordinate systems for each bone. Although standard methods for the development of coordinate systems for the 3-D measurement of bones and joint orientation have been reported for humans,[21,22] the evaluation of a deformity within a bone or joint requires the creation of several local coordinate systems within that bone or joint, including 1 proximal and 1 distal to the deformity.[20] Local 3-D coordinate systems for portions of long bones have been reported in multiple studies[20,23,24]; however, the descriptions of the methods used to identify angulation and rotation by means of CADS were succinct or absent in those studies. Little is known about the repeatability of geometric measurements of bones derived from CADS, and modeling software methods used to evaluate the geometry of canine long bones including the radius are not standardized or validated.

The purpose of the study reported here was to evaluate the repeatability and reliability of several methods that are based on common CADS practices and were used to assess the geometry of clinically normal (control) and deformed canine radii. We hypothesized that CADS methods would have a clinically acceptable within-subject repeatability of < 3° and a reliability > 0.75. We also hypothesized that, during evaluation of the proximal and distal aspects of the radius, a coordinate system that used points at the edge of the articular surface would be more repeatable and more reliable than a coordinate system that used a plane fit to the articular surface for both control and deformed radii. We further hypothesized that a coordinate system in which a cylinder was fit to the diaphyseal segment would be more repeatable and reliable than a coordinate system that was based on the centerline of that segment.

Materials and Methods

Samples

Computed tomographic scans of radii of dogs without (controls) and with unilateral or bilateral biapical radial deformities that were examined by the Orthopedic Surgery Service at the North Carolina State University Veterinary Hospital between July 2004 and March 2015 were considered for evaluation in the study. The electronic radiographic information system database was searched for potential CT scans, which were reviewed for study eligibility. Any CT scan that did not include the entire humerus and radius or had evidence of bone disease including fracture or neoplasia affecting the radius was excluded from the study. The body weight of the patient was not used as a criterion for study eligibility.

A convenience sampling method was used to select the CT scans that were evaluated in the study. Computed tomographic scans from all dogs with biapical radial deformities were evaluated, whereas CT scans for only 24 clinically normal radii (controls) were evaluated because of logistical limitations. For each CT scan evaluated in the study, the patient identification, sex, breed, and age at the time the scan was performed were recorded. The DICOM files of selected CT scans were imported into a commercially available CADS program.[a] Three-dimensional models were created in which the humerus and radius were separated and other bones were removed.

Humeral coordinate system

An x, y, and z Cartesian coordinate system was created relative to the humerus so that the x-axis was oriented medially-laterally, the y-axis was oriented cranially-caudally, and the z-axis was oriented proximally-distally **(Figure 1)**. A sphere was fit to the proximal articular surface of the humerus (ie, humeral head). The center of the sphere (HH) was selected as a landmark. Two additional landmarks were set at the lateral and medial epicondyles of the humerus, and a parallel reference line was drawn connecting those 2 landmarks (x-axis). The x-axis ran parallel to the elbow joint orientation line. The anatomic long axis of the humerus (z-axis) was determined by drawing a line through HH and the midpoint (CC) of the x-axis. A plane perpendicular to the z-axis was created (xy [transverse] plane) with the CC at its center; the plane was projected to include the landmarks at the lateral and medial epicondyles of the humerus. The xz (frontal) plane was created by selecting, in order, the CC, landmark at the lateral epicondyle of the humerus, and HH. The yz (sagittal plane) was a duplicate of the frontal plane except rotated 90° relative to the x-axis. The y-axis was the line created by the intersection of the transverse and sagittal planes. A point (y-point) was placed at the end of the line as a landmark for measurement purposes. Radial measurements were obtained relative to this humeral coordinate system.

Normalization of elbow joint extension

A cylinder was fit to the radius. The centerline of that cylinder was compared with the humeral z-axis (long axis of the humerus) to determine the angle of the elbow joint in the sagittal plane. The radius was rotated around the humeral x-axis to align the centerline of the cylinder and the humeral z-axis. The radius was sectioned into proximal, middle, and dis-

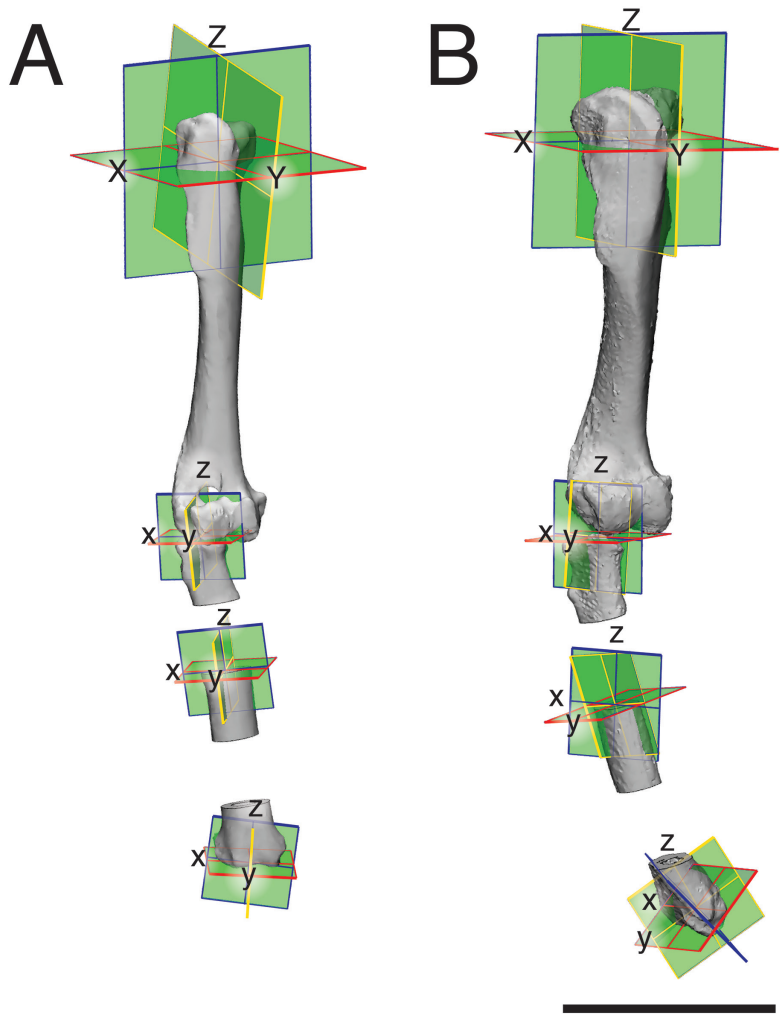

Figure 1—Representative 3-D reconstructed images derived from CT sequences of the right humerus and radius of a clinically normal dog (A) and a dog with a biapical radial deformity (B) overlaid with Cartesian coordinate systems for measurement of bone angulations derived from CADS. Each coordinate system consisted of 3 axes (x, y, and z) that were perpendicular to each other. The x-axis was oriented medially-laterally, the y-axis was oriented cranially-caudally, and the z-axis was oriented proximally-distally. The humeral coordinate system was based on 3 anatomic landmarks as described in the text and is depicted at the proximal portion of the bone in these illustrations for clarity. The frontal (xz) plane (blue edges) was defined by the x- and z-axes, the sagittal (yz) plane (yellow edges) was defined by the y- and z-axes, and the transverse (xy) plane (red edges) was defined by the x- and y-axes. The radius is depicted in 3 segments (proximal, diaphyseal, and distal) representing the top, middle, and bottom fifths of the bone. Each radial segment was fit with a Cartesian coordinate system that defined the frontal, sagittal, and transverse planes for that segment. As depicted here, the coordinate systems for the proximal and distal radial segments were determined by a BFA method, and the coordinate system for the diaphyseal segment was determined by a DPC method. For all radial segments, the frontal, sagittal, and transverse planes were defined and colored as described for those of the humeral coordinate system. Bar = 50 mm.

tal sections that represented 0% to 20%, 40% to 60%, and 80% to 100% of the length of the cylinder, respectively. The proximal and distal radial segments were used for epiphyseal measurements, and the middle radial segment was used for diaphyseal measurements. Each radial segment was fit with a Cartesian coordinate system so that the radial x-axes were oriented medially-laterally, the radial y-axes were oriented cranially-caudally, and the radial z-axes were oriented proximally-distally **(Figures 2 and 3)**.

BFA method for measurement of proximal and distal articular surfaces of the radius

Three different x, y, and z coordinate systems were created for each of the 3 radial segments. For the BFA method, the proximal and distal articular surfaces of the radius were individually marked. A plane was fit to each marked articular surface to serve as the BFA plane. Two reference points were placed at the most lateral and medial aspects of the marked articular surface and connected to form a temporary radial x-axis. A point was placed at the center of the temporary radial x-axis to serve as the origin for angle measurements (BFA-cc). The radial z-axis for each epiphyseal segment was created as a line originating from the BFA-cc that was perpendicular to the BFA plane. A radial z-point was placed at the end of the radial z-axis to serve as a landmark for measurements. The previously set lateral and medial reference points were projected onto the BFA plane and connected via BFA-cc to create a true radial x-axis that was perpendicular to the radial z-axis. A 3-point method was used to create the BFA planes for the proximal and distal epiphyseal segments of the radius. The BFA-cc, projected lateral point, and BFA radial z-point were selected to form the frontal plane of the radial segment. That plane was duplicated and rotated 90° around the x-axis to form the BFA transverse plane. The BFA sagittal plane was the plane that contained the BFA-cc and was perpendicular to the BFA frontal and transverse planes. The BFA y-axis was the line delineated by the intersection of the BFA transverse and sagittal planes. A reference point was set at the end of the line as the BFA y-point. Two-dimensional projection planes (sketch planes) of the 3 BFA planes were used for measurement of angulation in the frontal, sagittal, and transverse planes. Mediolateral angulation was measured as the angle between the radial-segment BFA z-axis and humeral z-axis in the frontal sketch plane. Craniocaudal angulation was measured as the angle between the radial-segment BFA z-axis and the humeral z-axis in the sagittal sketch plane. External-internal rotation angulation was measured as the angle between the radial-segment BFA y-axis and the humeral y-axis in the transverse sketch plane.

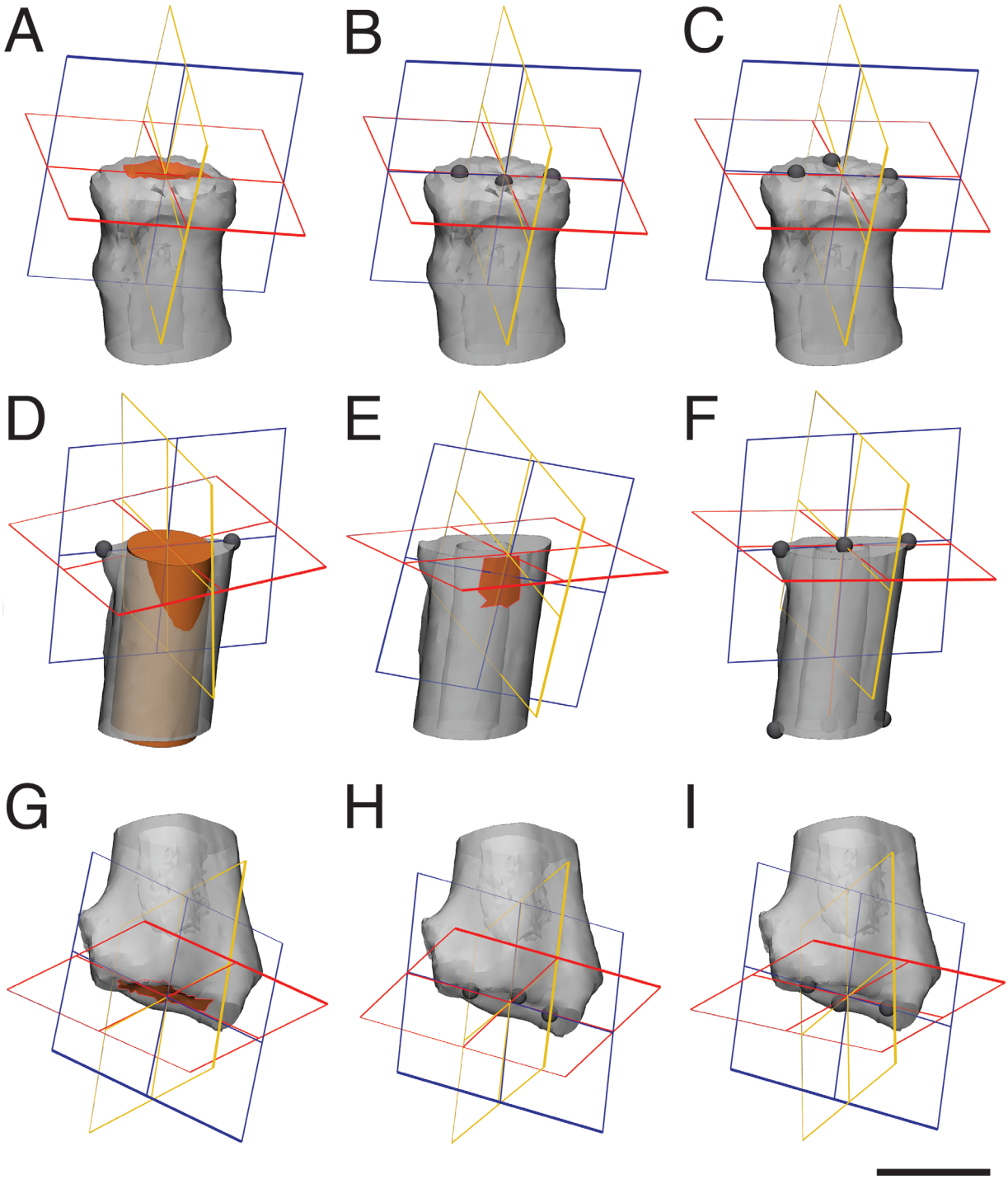

Figure 2—Representative 3-D reconstructed images derived from CT sequences of the proximal (A, B, and C), middle (diaphyseal; D, E, and F), and distal fifths (G, H, and I) of the right radius of the clinically normal dog of Figure 1 that depict the Cartesian coordinate systems for measurement of bone angulations by use of various CADS methods. The coordinate system for the proximal and distal radial segments was determined by a BFA (A and G), TLA-Cr (B and H), or TLA-Cd (C and I) method, and the coordinate system for the diaphyseal segment was determined by a BFC (D), STG (E), or DPC (F) method. The frontal (xz), sagittal (yz), and transverse (xy) planes are shown in blue, yellow, and red, respectively. Surfaces, cylinders, or axes used to create the coordinate systems are shown in orange. For the depicted radius, angular measurements of the proximal segment relative to humeral reference planes in the frontal, sagittal, and transverse planes were 3.34° (a positive value represents varus), 0.54° (a positive value represents procurvatum), and 45.34° (a positive value represents external rotation) in A; 3.92°, 0.57°, and 42.78° in B; and 3.92°, 0.11°, and 42.74° in C, respectively. Measurements of the diaphyseal segment in the frontal, sagittal, and transverse planes were 9.54°, 10.29°, and 42.04° in D; 6.94°, 3.60°, and 41.26° in E; and 2.51°, 0.69°, and 36.81° in F, respectively. Measurements of the distal segment in the frontal, sagittal, and transverse planes were 3.31°, 8.05°, and 30.39° in G; 4.11°, 5.61°, and 39.17° in H; and 4.15°, 9.77°, and 40.33° in I, respectively. Bar = 20 mm.

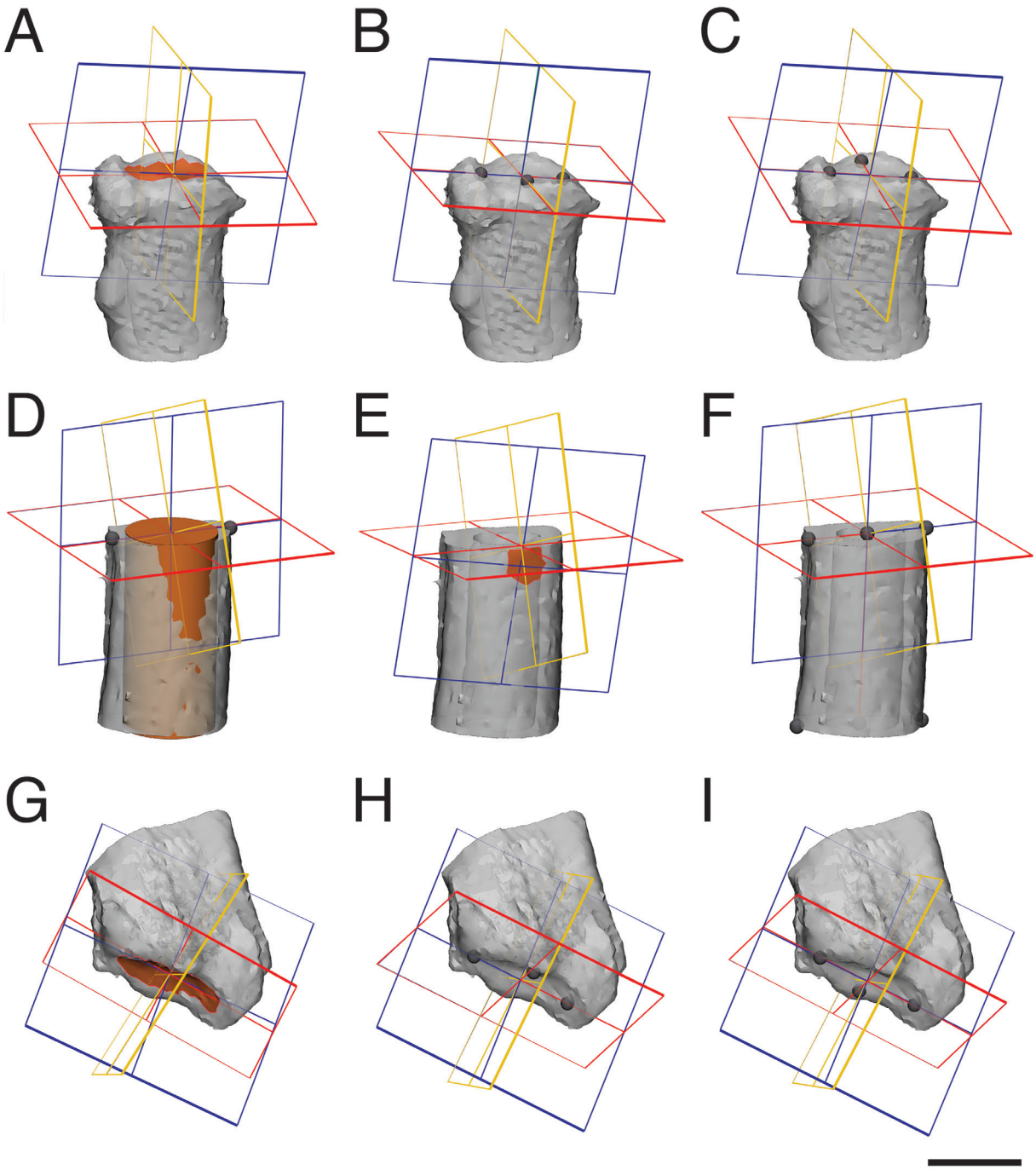

Figure 3—Representative 3-D reconstructed images derived from CT sequences of the proximal (A, B, and C), middle (diaphyseal; D, E, and F), and distal fifths (G, H, and I) of the right radius of the dog with a biapical radial deformity of Figure 1 that depict the Cartesian coordinate systems for measurement of bone angulations by use of CADS. For the depicted radius, measurements of the proximal segment in the frontal, sagittal, and transverse planes were 0.12°, 1.65°, and 62.25° in A; 2.00°, 6.09°, and 59.91° in B; and 1.99°, 1.77°, and 59.98° in C, respectively. Measurements of the diaphyseal segment in the frontal, sagittal, and transverse planes were 7.39°, 16.22°, and 82.48° in D; 6.04°, 16.14°, and 81.43° in E; and 10.62°, 11.87°, and 83.00° in F, respectively. Measurements of the distal segment in the frontal, sagittal, and transverse planes were 48.26°, 60.59°, and 67.11° in G; 48.69°, 56.73°, and 69.81° in H; and 51.22°, 60.63°, and 67.98° in I, respectively. ***See*** Figure 2 for remainder of key.

TLA method for measurement of proximal and distal articular surfaces of the radius

For the TLA method, reference points were placed at the most medial, cranial, lateral, and caudal aspects of the proximal and distal articular surfaces of the radius **(Figure 4)**. The articular surface was magnified to fill the screen, the point at which the medial aspect of the articular surface curved away from the transverse plane was identi-

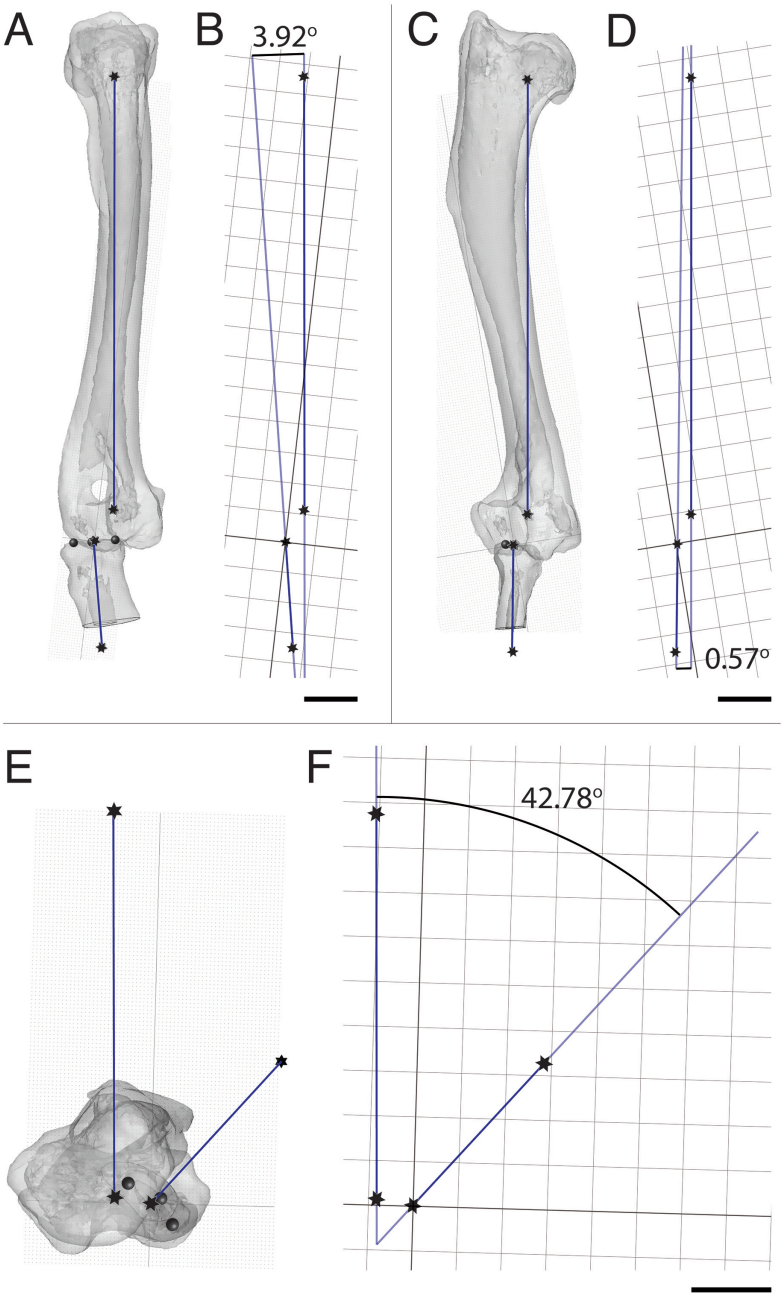

Figure 4—Representative 3-D reconstructed images derived from CT sequences of the right humerus and proximal fifth of the right radius from the cranial (A) and medial (C) aspects and the proximal articular surface of the right radius (E) for the clinically normal dog of Figure 1 and the corresponding CADS-derived, 2-D projected (sketch) planes (B, D and F) provided to demonstrate measurement of mediolateral (A and B), craniocaudal (C and D), and external-internal angulation (E and F) of the radius. The TLA-Cr method was used to create the depicted Cartesian coordinate system for the measurements. Mediolateral angulation was measured as the angle created at the intersection of the frontal planes of the radius and humerus (ie, intersection of the radial z-axis and humeral z-axis in the frontal [xz] sketch plane), and positive values were indicative of varus rotation. Craniocaudal angulation was measured as the angle created at the intersection of the sagittal planes of the radius and humerus (ie, intersection of the radial z-axis and the humeral z-axis in the sagittal [yz] sketch plane), and positive values were indicative of procurvatum. External-internal angulation was measured as the angle created at the intersection of the transverse and sagittal planes of the radius, and positive values were indicative of external rotation. In all panels, planes are depicted as blue lines with stars at each end. The respective angles for measurement were calculated by projection of the planes of interest onto a radial plane with the sketch plane function within the CADS. For the depicted normal radius, varus was 3.92° (B), procurvatum was 0.57° (D), and external rotation was 42.78° (F). Bars = 20 mm.

fied, and a reference point was placed adjacent to the start of curvature within the articular surface plane to mark the medial edge of that articular surface. The point automatically adhered (snapped) to the articular surface. That process was repeated to mark the lateral, cranial, and caudal aspects of the articular surface. A cranial plane that was defined by the cranial, lateral, and medial reference points was created (TLA-Cr method). A caudal plane that was defined by the caudal, medial, and lateral reference points was also created (TLA-Cd method). Lines perpendicular to the cranial and caudal planes were created and used to construct the z-axis for the radius, which represented the long axis of the bone segment for the TLA-Cr and TLA-Cd methods, respectively. Two sets of anatomic reference points were created for the TLA-Cr and TLA-Cd methods. These points were used to construct the radial x-axis parallel to the joint orientation and perpendicular to the radial z-axis. The radial y-axis was a line perpendicular to both the radial x-axis and radial z-axis. The frontal, sagittal, and transverse planes were created with the 3-perpendicular axes function. The mediolateral, craniocaudal, and external-internal rotation angulations were measured as described for the BFA method.

BFC method for measurement of the radial diaphysis

For the BFC method, a cylinder was fit to the diaphyseal segment of the radius. The cylinder axis was used to determine the anatomic long axis of the diaphyseal segment (z-axis). Reference points were set at the medial and lateral aspects of the edge of the cylinder where it contacted the reconstructed bone model. The x-axis was a line drawn perpendicular to the z-axis and parallel to the medial and lateral ref-

erence points. The frontal plane was constructed by use of reference points on the z- and x-axes. The transverse plane was created as the plane perpendicular to the frontal plane that contained the x-axis. The y-axis was the line perpendicular to both the x-axis and z-axis. The sagittal plane was created from points on the y-axis and z-axis. The mediolateral, craniocaudal, and external-internal rotation angulations were measured as described for the BFA method.

DPC method for measurement of the radial diaphysis

For the DPC method, 2 sets of reference points were placed on the lateral and medial aspects of both the proximal and distal aspects of the diaphyseal radial segment. The lateral and medial reference points at the proximal aspect of the diaphyseal radial segment were connected to create a temporary x-axis, as were the lateral and medial reference points at the distal aspect. Another reference point was placed at the midpoint of each temporary x-axis. The z-axis (long axis of the segment) was a line that connected the midpoints of the temporary x-axes. The frontal plane was constructed from the z-axis and center point of the proximal x-axis. The temporary x-axis was projected onto the frontal plane to create the true x-axis perpendicular to the z-axis. The y-axis was subsequently created perpendicular to both the x- and z-axes. The transverse plane was constructed perpendicular to the frontal plane from 3 points on the x- and z-axes. The sagittal plane was constructed perpendicular to the frontal and transverse planes. The mediolateral, craniocaudal, and external-internal rotation angulations were measured as described for the BFA method.

STG method for measurement of the radial diaphysis

For the STG method, a reference point was placed at the center of the cranioproximal surface of the radial segment, and the frontal plane was fit to the marked surface. The z-axis was drawn through the reference point within the frontal plane along the perceived long axis of the radial segment. Two anatomic reference points were marked on the lateral and medial aspects of the radial segment and projected onto the frontal plane. The transverse plane was constructed perpendicular to the frontal plane and parallel to the reference points on the lateral and medial aspects of the radial segment. The sagittal plane was constructed perpendicular to the frontal and transverse planes, and the y-axis was drawn perpendicular to the z-axis and frontal plane. The mediolateral, craniocaudal, and external-internal rotation angulations were measured as described for the BFA method.

Study measurements

For each radius, the x, y, and z measurements for the proximal and distal articular surfaces were obtained by use of the BFA, TLA-Cr, and TLA-Cd methods, and the x, y, and z measurements for the diaphysis were obtained by use of the BFC, DPC, and STG methods. All measurements were collected in random order and repeated 3 times with at least a 1-week interval between the repeated measurements. Thus, 81 measurements were recorded for each radius.

Statistical analysis

Radius was the observational unit for statistical analysis purposes, and each radius was considered an independent observation, even when both radii from a dog were evaluated. The data distribution for each CADS measurement method was assessed for normality by means of the Shapiro-Wilk test, and all measurement methods were found to be normally distributed ($P < 0.05$ and $W > 0.95$). Each measurement type was assessed by a 1-way ANOVA for repeated measures. Each model included a fixed effect for limb and a random effect to account for repeated measures within limbs. The within-subject repeatability (ie, repeatability of multiple measures on the same radius) was defined as the square root of the mean square error from the ANOVA (ie, model SD).[25] The intersubject repeatability was defined as the square root of the treatment mean square from the ANOVA (ie, treatment SD).[26,27,b]

Reliability was defined as the intraclass correlation coefficient and was calculated as follows: (intersubject variance)/(intersubject variance + within-subject variance), where the variances were obtained from the ANOVA. Values < 0.5 indicated poor reliability, between 0.5 and < 0.75 indicated moderate reliability, between 0.75 and < 0.9 indicated good reliability, and ≥ 0.9 indicated excellent reliability.[28]

Computer-aided design software methods with a within-subject repeatability < 3° and reliability > 0.75 were considered acceptable. Those were subjective criteria selected on the basis of our clinical experience and a review of the literature. The CVs (SD of replicates/mean of replicates) were used to analyze the repeatability of CADS methods and were calculated from the ANOVA. Methods with a CV < 20% were interpreted as being highly repeatable.[29] The mean bias and 95% limits of agreement between CADS methods when performing repeated measures within a limb were calculated by use of the Bland-Altman method as described.[30]

A CART[c] was used to predict which preset measurement criteria best classified radii as normal or abnormal.[31] For this analysis, all explanatory variables were considered until a binary division of a variable best reduced the deviance in the response (normal or abnormal). The mean of the 3 replicate measures for each measurement method was used for the CART analysis.

Results

Radii

Computed tomographic scans of 55 radii were evaluated; 24 radii from 16 dogs were considered clinically normal (control radii), and 31 radii from 18 dogs had a biapical deformity. The mean ± SD age was

5.4 ± 4.0 years (range, 0.9 to 13.4 years) for dogs with clinically normal radii and 1.3 ± 0.7 years (range, 0.5 to 3.1 years) for dogs with abnormal radii. A total of 4,455 angular measurements were collected (55 radii X 3 radial segments/radius X 3 coordinate systems/radial segment X 3 axes/coordinate system X 3 sets of measurements).

In control radii, the mean frontal plane angulation relative to the humerus was approximately 9° of varus at the proximal aspect of the radius, 6° of varus in the diaphysis, and 6° of varus at the distal aspect of the radius **(Table 1)**. This represented 3° of valgus angulation within the radius. In the sagittal plane, procurvatum was approximately 5° at the proximal aspect of the radius, 3° in the diaphysis, and 12° at the distal aspect of the bone for the 2 most consistent CADS methods. This represented 7° of procurvatum within the radius. In the transverse plane, external rotation was approximately 26° at the proximal aspect of the radius, 27° at the diaphysis, and 28° at the distal aspect of the radius. This represented 2° of external torsion within the radius.

In radii with biapical deformities, frontal plane angulation was approximately 13° of varus at the proximal aspect of the radius (4° more varus than control radii), 20° of varus in the diaphysis (14° more than control radii), and 25° of varus at the distal aspect of the radius (19° more than control radii) for the 2 most repeatable CADS methods. In the sagittal plane, procurvatum was approximately 9° at the proximal aspect of the radius (4° more procurvatum than control radii), 10° in the diaphysis (7° more than control radii), and 35° at the distal aspect of the radius (23° more than normal radii) for the 2 most consistent CADS methods. This represented 26° of procurvatum within the radius (19° more than control radii). In the transverse plane, external rotation was approximately 36° at the proximal aspect of the radius (10° more than control radii), 43° at the diaphysis (16° more than control radii), and 50° at the distal aspect of the radius (22° more than control radii). This represented 14° of external torsion within the radius (12° more than control radii).

In control radii, the mean ± SD within-subject repeatability of radial angular measurements for all methods was 1.40 ± 0.67° (range, 0.76° to 2.97°) in the frontal plane, 3.17 ± 2.21° (range, 0.69° to 6.68°) in the sagittal plane, and 3.01 ± 1.11° (range, 1.72° to 5.31°) in the transverse plane **(Table 2)**. The mean ± SD reliability of radial measurement methods was 0.94 ± 0.07 (range, 0.76 to 0.97) in the frontal plane, 0.83 ± 0.10 (range, 0.67 to 0.95) in the sagittal plane, and 0.95 ± 0.06 (range, 0.82 to 0.99) in the transverse plane. In abnormal radii, the mean ± SD within-subject repeatability of radial angular measurements for all methods was 2.56 ± 1.95° (range, 0.42° to 6.12°) in the frontal plane, 3.59 ± 2.39° (range, 1.24° to 6.91°) in the sagittal plane, and 3.47 ± 1.19° (range, 2.06° to 5.49°) in the transverse plane **(Table 3)**. The mean ± SD reliability of radial measurement methods was 0.98 ± 0.01 (range, 0.96 to 1.00) in the frontal plane, 0.97 ± 0.05 (range, 0.83 to 1.00) in the sagittal plane, and 0.98 ± 0.01 (range, 0.96 to 0.99) in the transverse plane. The median CV was 15.4% (range, 6.19% to 74.77%) in control radii and 10.1% (range, 2.04% to 56.16%) in abnormal radii. The CV was > 20% for 19 of 54 angular measurements (12 of 27 measure-

Table 1—Mean ± SD values for 3-D geometric measurements of 24 clinically normal radii from 16 dogs and 31 radii with biapical deformities from 18 dogs as determined from the application of various CADS methods to 3-D reconstructed images derived from CT sequences.

Radius type	Radial segment	CADS measurement method	Mediolateral angulation (°)*	Craniocaudal angulation (°)†	External-internal rotation angulation (°)‡
Normal	Proximal	BFA	9.71 ± 1.00	2.89 ± 1.36	27.83 ± 5.31
		TLA-Cr	9.27 ± 1.19	8.34 ± 5.88	25.98 ± 3.82
		TLA-Cd	9.14 ± 1.13	4.73 ± 2.82	25.93 ± 3.70
	Diaphyseal	BFC	6.17 ± 0.88	2.08 ± 1.37	27.78 ± 1.72
		DPC	6.09 ± 0.76	2.48 ± 0.69	27.43 ± 2.09
		STG	5.29 ± 2.97	2.90 ± 2.17	26.22 ± 2.83
	Distal	BFA	5.35 ± 1.34	14.40 ± 2.21	27.65 ± 2.40
		TLA-Cr	5.63 ± 1.59	9.20 ± 5.36	26.52 ± 2.36
		TLA-Cd	6.18 ± 1.76	24.95 ± 6.68	29.37 ± 2.88
Biapical deformity	Proximal	BFA	13.55 ± 0.94	6.85 ± 1.63	35.55 ± 3.60
		TLA-Cr	12.53 ± 1.18	11.65 ± 6.55	35.02 ± 3.50
		TLA-Cd	12.68 ± 1.09	9.55 ± 3.19	33.98 ± 4.41
	Diaphyseal	BFC	20.71 ± 1.64	11.52 ± 2.40	42.93 ± 2.07
		DPC	20.39 ± 0.42	11.93 ± 1.24	43.10 ± 2.06
		STG	19.01 ± 4.12	7.28 ± 1.56	44.21 ± 2.39
	Distal	BFA	27.43 ± 4.15	41.70 ± 2.22	53.44 ± 3.16
		TLA-Cr	23.17 ± 3.36	27.98 ± 6.60	46.96 ± 4.51
		TLA-Cd	34.03 ± 6.12	53.94 ± 6.91	59.42 ± 5.49

The proximal, diaphyseal, and distal radial segments represented the proximal, middle, and distal fifths of the bone, respectively.

*Measured in the frontal plane; positive values represent varus. †Measured in the sagittal plane; positive values represent procurvatum. ‡Measured in the transverse plane; positive values represent external rotation.

Table 2—Within-subject and intersubject repeatability, reliability, and CV for various CADS measurement methods when applied to the 24 clinically normal radii described in Table 1.

Radial segment	CADS measurement method	Plane	Within-subject repeatability: For the described plane (°)	Within-subject repeatability: Mean for all 3 planes combined (°)	Intersubject repeatability (°)	Reliability	CV (%)
Proximal	BFA	Frontal	1.00	2.56	5.66	0.97	10.3
		Sagittal	1.36		4.01	0.90	47.2
		Transverse	5.31		11.24	0.82	19.1
	TLA-Cr	Frontal	1.19	3.63	6.14	0.96	12.8
		Sagittal	5.88		9.72	0.73	70.6
		Transverse	3.82		13.41	0.92	14.7
	TLA-Cd	Frontal	1.13	2.55	5.94	0.96	12.4
		Sagittal	2.82		7.78	0.88	59.7
		Transverse	3.70		13.69	0.93	14.3
Diaphyseal	BFC	Frontal	0.88	1.32	5.01	0.97	14.3
		Sagittal	1.37		2.55	0.78	65.9
		Transverse	1.72		13.94	0.99	6.2
	DPC	Frontal	0.76	1.18	4.73	0.97	12.4
		Sagittal	0.69		2.52	0.93	27.9
		Transverse	2.09		14.16	0.98	7.6
	STG	Frontal	2.97	2.66	5.32	0.76	56.1
		Sagittal	2.17		4.54	0.81	74.8
		Transverse	2.83		12.86	0.95	10.8
Distal	BFA	Frontal	1.34	1.98	5.75	0.95	25.0
		Sagittal	2.21		9.72	0.95	15.4
		Transverse	2.40		19.40	0.98	8.7
	TLA-Cr	Frontal	1.59	3.10	6.64	0.95	28.3
		Sagittal	5.36		7.63	0.67	58.2
		Transverse	2.36		19.66	0.99	8.9
	TLA-Cd	Frontal	1.76	3.77	7.19	0.94	28.4
		Sagittal	6.68		10.83	0.72	26.8
		Transverse	2.88		21.34	0.98	9.8

See Table 1 for remainder of key.

ments in control radii and 7 of 27 measurements in abnormal radii). Of the 19 CVs that were > 20%, 14 were for the assessment of craniocaudal angulation, and 5 were for the assessment of mediolateral angulation; the CV was not > 20% for any external-internal rotation angulation measurement. Subjectively, the CV was larger when the mean measurement was smaller. The mean ± SD bias between CADS-based radial measurement methods was 1.88 ± 2.07° (range, 0.22° to 6.36°) in the frontal plane, 6.44 ± 6.80° (range, 0.41° to 21.51°) in the sagittal plane, and 2.27 ± 2.81° (range, 0.04° to 8.27°) in the transverse plane **(Table 4)**.

During the CART analyses, the most predictive tree for distinguishing between control and abnormal radii combined 2 nodes (whether the craniocaudal angulation of the distal portion of the radius [distal radial procurvatum] relative to the long axis of the antebrachium was > 30.54° and, when the distal radial procurvatum was ≤ 30.54°, whether the external rotation of the radial diaphysis was > 30.69°). Thirty of 32 radii with a distal radial procurvatum > 30.54° were abnormal. Six of 7 radii with a distal radial procurvatum ≤ 30.54° and external rotation of the radial diaphysis > 30.69° were clinically normal, and all 16 radii with a distal radial procurvatum ≤ 30.54° and external rotation of the radial diaphysis ≤ 30.69° were clinically normal. The described 2-node combination had a sensitivity of 97% and specificity of 92% for identification of biapical radial deformity.

Discussion

In dogs, radial deformities are common, and biapical radial deformities are reportedly twice as common as uniapical radial deformities.[32] Assessment of angulation and torsion in radii with biapical deformities is complex because correlation is poor among clinical, radiographic, and CT measurements[33]; this fact suggests that those measurement methods lack precision. The use of CADS for 3-D assessment and surgical planning for correction of biapical radial deformities requires the creation of 3-D coordinate systems (ie, methods) aligned with the proximal, diaphyseal, and distal portions of the bone. In the present study, several different local coordinate systems for those 3 segments of the radius were developed and applied by CADS to CT scans of dogs with clinically normal (control) radii and radial deformities that were perceived to be biapical in nature on initial clinical evaluation. Development of the local coordinate systems involved the construction of lines or planes on the basis of anatomic features in a process described as the creation of user-defined landmarks, which is common for measurement of bones

Table 3—Within-subject and intersubject repeatability, reliability, and CV for various CADS measurement methods when applied to the 31 radii with biapical deformities described in Table 1.

Radial segment	CADS measurement method	Plane	Within-subject repeatability: For the described plane (°)	Within-subject repeatability: Mean for all 3 planes combined (°)	Intersubject repeatability (°)	Reliability	CV (%)
Proximal	BFA	Frontal	0.94	2.06	11.96	0.99	7.0
		Sagittal	1.63		14.07	0.99	23.8
		Transverse	3.6		23.10	0.98	10.1
	TLA-Cr	Frontal	1.18	3.74	11.54	0.99	9.4
		Sagittal	6.55		14.32	0.83	56.2
		Transverse	3.50		22.28	0.98	10.0
	TLA-Cd	Frontal	1.09	2.89	12.58	0.99	8.6
		Sagittal	3.19		18.40	0.97	33.4
		Transverse	4.41		21.64	0.96	13.0
Diaphyseal	BFC	Frontal	1.64	2.04	21.88	0.99	7.9
		Sagittal	2.40		18.01	0.98	20.8
		Transverse	2.07		20.90	0.99	4.8
	DPC	Frontal	0.42	1.24	20.42	1.00	2.0
		Sagittal	1.24		18.98	1.00	10.4
		Transverse	2.06		20.77	0.99	4.8
	STG	Frontal	4.12	2.69	19.83	0.96	21.7
		Sagittal	1.56		13.67	0.99	21.4
		Transverse	2.39		22.46	0.99	5.4
Distal	BFA	Frontal	4.15	3.18	35.60	0.99	15.1
		Sagittal	2.22		32.00	1.00	5.3
		Transverse	3.16		34.18	0.99	5.9
	TLA-Cr	Frontal	3.36	4.82	29.76	0.99	14.5
		Sagittal	6.60		30.66	0.96	23.6
		Transverse	4.51		34.17	0.98	9.6
	TLA-Cd	Frontal	6.12	6.17	36.34	0.97	18.0
		Sagittal	6.91		30.23	0.95	12.8
		Transverse	5.49		35.66	0.98	9.2

See Table 1 for remainder of key.

Table 4—Mean bias (95% limits of agreement) between various CADS measurement methods when applied to the clinically normal and abnormal radii described in Table 1.

Radial segment	CADS measurement methods compared	Mediolateral angulation	Craniocaudal angulation	External rotation angulation
Proximal	TLA-Cr and BFA	–0.77 (–4.91 to 3.37)	5.08 (–8.63 to 18.79)	–1.11 (–8.84 to 6.62)
	TLA-Cd and BFA	–0.78 (–8.48 to 6.92)	2.23 (–6.94 to 11.40)	–1.71 (–9.02 to 5.60)
	TLA-Cd and TLA-Cr	–0.01 (–7.26 to 7.24)	–2.76 (–19.74 to 14.22)	–0.61 (–3.91 to 2.69)
Diaphyseal	DPC and BFC	–0.22 (–5.64 to 5.20)	0.41 (–4.64 to 5.46)	–0.06 (–2.87 to 2.75)
	STG and BFC	–1.35 (–17.71 to 15.01)	–2.03 (–11.05 to 6.99)	0.04 (–8.17 to 8.25)
	STG and DPC	–1.13 (–15.19 to 12.93)	–2.44 (–12.20 to 7.32)	0.10 (–7.57 to 7.77)
Distal	TLA-Cr and BFA	–2.28 (–15.99 to 11.43)	–10.00 (–27.02 to 7.02)	–4.15 (–17.82 to 9.52)
	TLA-Cd and BFA	4.08 (–8.24 to 16.40)	11.51 (–5.05 to 28.07)	4.12 (–9.30 to 17.54)
	TLA-Cd and TLA-Cr	6.36 (–12.06 to 24.78)	21.51 (–0.56 to 43.58)	8.27 (–14.04 to 30.58)

See Table 1 for remainder of key.

with CADS.[12,13,24,34] The repeatability and reliability of these methods were evaluated in control and abnormal radii.

To mitigate the effect of elbow joint angulation on measurements of procurvatum, the radius was rotated relative to the x-axis (lateromedial axis) of the humerus before measurements of the proximal radial segment were obtained. Because the goal of that rotation was to normalize extension of the elbow joint, the orientation of the radius was corrected on the basis of the long axis of the humerus (humeral z-axis) and long axis of the radius (ie, the centerline of a cylinder fit to the radius). Alternative methods could have been considered for normalization of elbow joint extension. The radius could have been rotated on the basis of the orientation of its proximal articular surface, but that would have interfered with measurements that were based on that surface. The decision to align the radius on the basis of the centerline of a cylinder fit to it affected procurvatum measurements. The fact that all procurvatum measurements had positive values (ie, all radial segments were caudally oriented) suggested that the CADS methods used appropriately described procurvatum.

However, procurvatum measurements were likely influenced by the procurvatum present within each bone because each bone was rotated along its long axis. The veterinary literature lacks clear information on where procurvatum originates in normal and deformed radii. Thus, orientation of the radius along its long axis rather than on the basis of its proximal articular surface led to an underestimation of procurvatum for each of the 3 radial segments. Consequently, the procurvatum measurements reported in the present study should be interpreted with caution and are not interchangeable with procurvatum measurements that are based on the orientation of the proximal articular surface of the radius, such as the center of rotation of angulation method.[3]

In the present study, angular measurements were obtained with the CADS by projecting axes on planes. A decision was made to project the corresponding radial and humeral axes onto radial planes rather than onto humeral planes. Although the use of humeral planes instead of radial planes did not appear to change measurements during the development of the analytic methods used in the present study, the interchangeability of radial and humeral planes was not systematically evaluated. It is possible that the angular measurements evaluated in this study would have differed had the corresponding radial and humeral axes been projected onto humeral planes. The angulation measurements reported in the present study should not be directly compared with angulation measurements obtained by use of other methods. Nevertheless, the use of radial planes to measure radius angulation was unlikely to have influenced the repeatability and reliability of the reported measurements.

Most methods described in the present study had acceptable repeatability and good or excellent reliability. Thus, we accepted (or failed to reject) our hypothesis that the use of CADS to evaluate the 3-D geometry of the canine radius yielded repeatable and reliable measurements. For the proximal portion of the radius, the repeatability and reliability of the methods that fit a plane to the articular surface and placed landmarks at the caudal, medial, and lateral aspects of the articular surface were numerically superior for both control and abnormal radii. In human medicine, the construction of coordinate systems to evaluate articular surfaces of bones is similarly based on establishing user-defined anatomic landmarks at the edges of[23,35] and fitting geometric shapes to[12,13,36] those surfaces. For both control and abnormal radii, the repeatability and reliability of diaphyseal measurements were numerically superior for the method that fit a cylinder to the diaphysis and the method that calculated the centerline of the bone. Thus, we rejected our hypothesis that a coordinate system created by fitting a cylinder to the diaphyseal segment was more repeatable and reliable than a coordinate system based on the centerline of that bone segment. Centerlines have been used to analyze the diaphysis of long bones[12,37] and can be straight or curved (ie, arc or freeform centerlines).[37–40] In the present study, a straight centerline based on the proximal and distal aspects of the diaphysis was used. It remains unclear whether an arc centerline would provide more repeatable or reliable measurements of the radial diaphysis than a straight centerline. For the distal portion of the radius, repeatability and reliability were numerically superior for the methods that fit a plane to the articular surface and placed landmarks at the cranial, medial, and lateral aspects of the articular surface for both control and abnormal radii. The method that placed landmarks at the caudal, medial, and lateral aspects of the articular surface was less repeatable and overestimated varus, procurvatum, and external rotation angulation, compared with the other methods. Because the 2 methods based on 3 articular surface landmarks had the medial and lateral landmarks in common, bias in the caudal method was the result of the fact that the landmark placed at the caudal aspect of the distal articular surface did not accurately represent that surface. This was particularly evident in radii with biapical deformities where the bias in procurvatum was ≥ 10°. Because the repeatability was acceptable for all measurements of the proximal and distal portions of the radius in the present study, we rejected our hypothesis that coordinate systems based on landmarks at the edges of the articular surface (TLA-Cr and TLA-Cd methods) would be more repeatable and reliable than a coordinate system based on a plane fit to the articular surface (BFA method). In the present study, the CVs were relatively small for all methods and were numerically larger when angles were smaller. This was likely because, when measurements are obtained with equal precision, similar errors represent a larger proportion of small angles than large angles. Regardless, the accuracy (repeatability and reliability) of angular measurements of canine radii obtained by use of CADS in the present study was comparable to that of other methods used to evaluate the angulation of bones.

The accuracy of bone angulation measurement by use of external methods (goniometry or kinematic analysis) and medical imaging (radiography, fluoroscopy, or CT) has been described in the medical literature. Results of a study[41] involving 28 human patients with a hammertoe deformity (ie, dorsiflexion of the metatarsophalangeal joint, plantarflexion of the proximal interphalangeal joint, and either normal position or dorsiflexion at the distal interphalangeal joint) indicate that the bias and within-subject repeatability for goniometric measurements were 1.93° and 2.15°, respectively, when compared with measurements obtained by use of a coordinate-measuring machine (gold standard). During kinematic analyses of human subjects, the within-subject repeatability of measurements in the sagittal, transverse, and frontal planes for 4 foot segments ranged from 0.57° to 1.95° (median repeatability for all measurements, 0.70°).[42] In a study[43] in which tibial torsion in 10 human subjects

was evaluated by use of 2 fluoroscopic devices, the reproducibility reported for both devices was 1.3°, the calculated bias was –0.08° and 1.01°, and the within-subject repeatability was 0.58° and 0.76°. In a study[44] in which 3 radiographic methods to evaluate the tibial plateau in 130 dogs were compared, the repeatability of measurements among 6 observers ranged from 3.13° to 4.07° (median repeatability for all measurements, 3.53°). In a study[45] in which 14 femoral and tibial angular measurements were obtained from radiographic images to evaluate hind limb alignment in 12 Chihuahuas, the repeatability of those measurements ranged from 1.76° to 4.33° (median repeatability for all measurements, 3.90°), and the reproducibility (ie, interobserver variability) ranged from 2.74° to 8.57° (median, 5.56°). In a study[46] in which the patellar ligament angle was measured on radiographic images for 87 dogs, the within- and between-observer repeatability for 3 observers ranged from 5.29° to 5.53°, and reproducibility (ie, SD of measurements among observers) ranged from 5.16° to 5.31°. In a study[47] conducted to evaluate the accuracy of 3 radiographic views for measurement of the hip-knee angle in 50 human subjects, the mean bias calculated from supplementary data was –0.64°, –0.03°, and 0.83°, and the within-subject repeatability was 0.17°, 0.27°, and 0.53° for the respective views. In a study[48] involving children with femoral fractures, radiographic measurement of femoral alignment had a reproducibility that ranged from 1.7° to 2.6°. In a study[23] conducted to assess the orientation of the distal articular surface of the radius in human subjects, the within-subject repeatability of 3-D angular measurements derived from reconstructed CT images as estimated from the data was 0.28° and the estimated reproducibility was 0.13°. Those values were superior to the estimated within-subject repeatability of measurements derived from radiographic images (2.72°).[23] In a study[49] that evaluated hind limb alignment in 20 dogs by means of 5 femoral and tibial angular measurements derived from multiplanar reconstructed CT images, the estimated mean repeatability ranged from 1.19° to 3.00° (median repeatability for all 5 measurements, 1.73°), and the estimated mean reproducibility ranged from 1.74° to 3.71° (median reproducibility for all 5 measurements, 2.87°). In another study[3] in which measurements of canine femurs were derived from 3-D reconstructed CT images, the intraobserver repeatability was 2.4° and 2.6° for 2 observers, and reproducibility was 3.5°. When considered collectively, the medical literature indicates that measurements of bone angulation have small bias and high repeatability. Also, as expected, measurements obtained from CT images appear to be more repeatable than measurements obtained from radiographic images.

In the present study, the angulation for control radii was 3° of valgus, 7° of procurvatum, and 2° of external torsion. The overall variability (ie, repeatability between subjects) in angulation was small for the control radii. The variability for angulation in the frontal and sagittal planes was smaller than that for the external-internal rotation plane, most likely because the limbs were scanned at various degrees of antebrachial supination, and supination leads to external rotation of the radius. The angulation for the control radii evaluated in the present study was comparable to the mean valgus (2.7°) and procurvatum (25.2°) derived from radiographic images for 20 clinically normal canine radii of another study.[3] However, it is important to note that the angulation values reported in the present study should not be directly compared with angulation values that were derived by use of other methods. This is particularly relevant for procurvatum because, in the present study, we altered the extension of the elbow joint along the long axis of the radius, and changing the orientation of the elbow joint affects procurvatum measurements. In a previous report,[3] measurements of procurvatum were made solely on the basis of the orientation of the proximal articular surface of the radius rather than the long axis of the bone. For the abnormal radii evaluated in the present study, the angulation was 7° of varus in the diaphysis relative to the proximal portion of the bone, 5° of varus in the distal portion of the bone relative to the diaphysis, 26° of procurvatum, and 14° of external torsion. The finding that varus angulation was larger at the distal portion of the radius relative to the radial diaphysis was unexpected and is counterintuitive because the dogs selected for enrollment appeared to have biapical radial deformities at the time of initial evaluation. Biapical radial deformities generally include varus angulation of the proximal portion of the radius and valgus angulation of the distal aspect of the antebrachium.[33] The presence of external rotation and procurvatum potentially altered the clinical perception of valgus angulation of the distal portion of the radius at the time of initial clinical assessment, just as external rotation influences measurement of valgus angulation on radiographic images and procurvatum influences measurement of radial torsion on CT images.[6,50] The findings of the present study warrant further investigation. In a case-series report[33] of 13 dogs with biapical radial deformities that were measured by the use of multiplanar reconstructed CT images, the mean ± SD radial procurvatum was 46 ± 10° and external torsion was 33 ± 17°. The discrepancies in radial procurvatum and torsion measurements between the present study and that case-series report[33] were likely caused by differences in the methods used to measure angles on the multiplanar reconstructed CT images and by the CADS. These differences also require further investigation.

The accuracy of the methods used to measure angulation of the radial segments was not evaluated in the present study because a gold standard method has not been established. The presence of bias between measurements acquired by the use of different CADS methods suggested that the methods used should be specifically described when CADS-derived measure-

ments of bone angulation are reported. Additionally, sources of bias in angulation measurements should be investigated further. Because the CADS methods used in the present study were applied to CT images, the results were dependent on the accuracy of the CT sequences. Results of a study[34] conducted to assess the accuracy of CT sequencing of the distal portion of the radius of cats indicate that deviations from articular surfaces are approximately half the width of reconstructed CT slices. If it is assumed that a similar error was present in the CT scans used in the present study, the angular inaccuracy of a CADS-based rendering of a 20-mm-wide radius acquired with a CT slice thickness of 1 mm would be within ± 1.4° at each end of the bone. Determination of the reproducibility (ie, interobserver repeatability) of the CADS methods described in the present study was not possible because all measurements were obtained by 1 investigator. Findings of other studies[49,d] suggest that, in dogs, the reproducibility of varus measurements of the femur and tibia derived from reconstructed CT images was approximately 50% greater than the corresponding repeatability of those measurements. Therefore, it seems logical to estimate that the reproducibility of the CADS methods described in the present study would be slightly greater than the reported repeatability.

The CADS methods described in the present study could be clinically useful for planning correction of radial deformities.[18,20,51] The described methods can also be incorporated into the automation of angular measurements for bones. Results of other studies[23,52] indicate that automated 3-D assessment methods for bones are rapid and precise; readings took 30 to 40 seconds and intraobserver repeatability was < 1°. The CART analysis described in the present study was highly sensitive and specific for detection of radial deformities and used 1 node (threshold) of angulation and 1 node of rotation. Classification and regression tree analysis is practical and could be clinically useful for screening patients for the presence of a radial deformity, determining the need for correction of a deformity, and selecting the amplitude of the correction.

In the present study, CADS-based methods to measure the 3-D orientation of the proximal, diaphyseal, and distal segments of the radius in dogs were described. Results indicated that those methods were repeatable and reliable for evaluation of both normal and abnormal radii.

Acknowledgments

Supported in part by the Morris Animal Foundation (grant No. D16CA-620).

The authors declare that there were no conflicts of interest.

The authors thank Drs. Ola L. A. Harrysson and Caroline E. Webster and Ms. Amanda L. Bell and Sara E. Russell at North Carolina State University, Raleigh, NC, for technical assistance and Dr. Chrisoula Toupadakis Skouritakis for the illustrations.

Footnotes

a. Mimics Creative Suite featuring Mimics 17.0 and 3-matic 9.0, Materialise, Plymouth, Mich.

b. SAS, version 9.4, SAS Institute, Cary, NC.

c. Partykit package and ctree function, R: a language and environment for statistical computing, version 1.2-11, R Foundation for Statistical Computing, Vienna, Austria. Available at: www.R-project.org. Accessed Jun 16, 2020.

d. Miles JE, Berg-Sørensen K, Buelund LE. Can CT measurements of femoral varus be performed reliably—even between reconstructions? (abstr), in *Proceedings*. Br Sm Anim Vet Assoc Cong 2015;58.

References

1. Lewis DD, Radasch RM, Beale BS, et al. Initial clinical experience with the IMEX circular external skeletal fixation system. Part II. Use in bone lengthening and correction of angular and rotational deformities. *Vet Comp Orthop Traumatol* 1999;12:118–127.
2. Balfour RJ, Boudrieau RJ, Gores BR. T-plate fixation of distal radial closing wedge osteotomies for treatment of angular limb deformities in 18 dogs. *Vet Surg* 2000;29:207–217.
3. Fox DB, Tomlinson JL, Cook JL, et al. Principles of uniapical and biapical radial deformity correction using dome osteotomies and the center of rotation of angulation methodology in dogs. *Vet Surg* 2006;35:67–77.
4. Dismukes DI, Fox DB, Tomlinson JL, et al. Determination of pelvic limb alignment in the large-breed dog: a cadaveric radiographic study in the frontal plane. *Vet Surg* 2008;37:674–682.
5. Breiteneicher AH, Norby B, Schulz KS, et al. The effect of sliding humeral osteotomy (SHO) on frontal plane thoracic limb alignment: an ex vivo canine cadaveric study. *Vet Surg* 2016;45:1095–1107.
6. Piras LA, Peirone B, Fox D. Effects of antebrachial torsion on the measurement of angulation in the frontal plane: a cadaveric radiographic analysis. *Vet Comp Orthop Traumatol* 2012;25:89–94.
7. Stevens PM. Radiographic distortion of bones: a marker study. *Orthopedics* 1989;12:1457–1463.
8. Husmann O, Rubin PJ, Leyvraz PF, et al. Three-dimensional morphology of the proximal femur. *J Arthroplasty* 1997;12:444–450.
9. Ravaud P, Giraudeau B, Auleley GR, et al. Variability in knee radiographing: implication for definition of radiological progression in medial knee osteoarthritis. *Ann Rheum Dis* 1998;57:624–629.
10. Walch G, Mesiha M, Boileau P, et al. Three-dimensional assessment of the dimensions of the osteoarthritic glenoid. *Bone Joint J* 2013;95-B:1377–1382.
11. Eckhoff DG, Bach JM, Spitzer VM, et al. Three-dimensional mechanics, kinematics, and morphology of the knee viewed in virtual reality. *J Bone Joint Surg Am* 2005;87(suppl 2):71–80.
12. Smith EJ, Marcellin-Little DJ, Harrysson OLA, et al. Three-dimensional assessment of curvature, torsion, and canal flare index of the humerus of skeletally mature nonchondrodystrophic dogs. *Am J Vet Res* 2017;78:1140–1149.
13. Dunlap AE, Mathews KG, Walters BL, et al. Three-dimensional assessment of the influence of juvenile pubic symphysiodesis on the pelvic geometry of dogs. *Am J Vet Res* 2018;79:1217–1225.
14. Agarwal M, Puri A, Gulia A, et al. Joint-sparing or physeal-sparing diaphyseal resections: the challenge of holding small fragments. *Clin Orthop Relat Res* 2010;468:2924–2932.
15. Sporer SM, Della Valle C. Porous metal augments: big hopes for big holes. *Orthopedics* 2010;33:651.
16. Worth AJ, Crosse KR, Kersley A. Computer-assisted surgery using 3D printed saw guides for acute correction of antebrachial angular limb deformities in dogs. *Vet Comp Orthop Traumatol* 2019;32:241–249.
17. Hall EL, Baines S, Bilmont A, et al. Accuracy of patient-specific three-dimensional-printed osteotomy and reduction guides for distal femoral osteotomy in dogs with medial patella luxation. *Vet Surg* 2019;48:584–591.
18. Dobbe JG, du Pré KJ, Kloen P, et al. Computer-assisted and patient-specific 3-D planning and evaluation of a single-cut

rotational osteotomy for complex long-bone deformities. *Med Biol Eng Comput* 2011;49:1363–1370.
19. Zheng GS, Su YX, Liao GQ, et al. Mandible reconstruction assisted by preoperative simulation and transferring templates: cadaveric study of accuracy. *J Oral Maxillofac Surg* 2012;70:1480–1485.
20. Domenech L, Munoz-Almaraz FJ, Serra CI, et al. A 3D mathematical model for planning ostectomy on long-bone angular deformities. *J Comput Appl Math* 2016;291:58–65.
21. Wu G, Siegler S, Allard P, et al. ISB recommendation on definitions of joint coordinate system of various joints for the reporting of human joint motion—part I: ankle, hip, and spine. International Society of Biomechanics. *J Biomech* 2002;35:543–548.
22. Wu G, van der Helm FC, Veeger HE, et al. ISB recommendation on definitions of joint coordinate systems of various joints for the reporting of human joint motion—part II: shoulder, elbow, wrist and hand. *J Biomech* 2005;38:981–992.
23. Nysjö J, Christersson A, Sintorn I-M, et al. Precise 3D angle measurements in CT wrist images, in *Proceedings*. Int Conf Image Anal Process 2013;479–488.
24. Miranda DL, Rainbow MJ, Leventhal EL, et al. Automatic determination of anatomical coordinate systems for three-dimensional bone models of the isolated human knee. *J Biomech* 2010;43:1623–1626.
25. Bartlett JW, Frost C. Reliability, repeatability and reproducibility: analysis of measurement errors in continuous variables. *Ultrasound Obstet Gynecol* 2008;31:466–475.
26. McAlinden C, Khadka J, Pesudovs K. Precision (repeatability and reproducibility) studies and sample-size calculation. *J Cataract Refract Surg* 2015;41:2598–2604.
27. Barnhart HX, Barboriak DP. Applications of the repeatability of quantitative imaging biomarkers: a review of statistical analysis of repeat data sets. *Transl Oncol* 2009;2:231–235.
28. Portney LG. *Foundations of clinical research: applications to evidence-based practice*. 4th ed. Upper Saddle River, NJ: Prentice Hall, 2020;486–491.
29. Assam PN, Mintiens K, Knapen K, et al. Estimating precision, repeatability, and reproducibility from Gaussian and non-Gaussian data: a mixed models approach. *J Appl Stat* 2010;37:1729–1747.
30. Bland JM, Altman DG. Agreement between methods of measurement with multiple observations per individual. *J Biopharm Stat* 2007;17:571–582.
31. Lawrence RL, Wright A. Rule-based classification systems using classification and regression tree (CART) analysis. *Photogramm Eng Remote Sensing* 2001;67:1137–1142.
32. Knapp JL, Tomlinson JL, Fox DB. Classification of angular limb deformities affecting the canine radius and ulna using the center of rotation of angulation method. *Vet Surg* 2016;45:295–302.
33. Kwan TW, Marcellin-Little DJ, Harrysson OL. Correction of biapical radial deformities by use of bi-level hinged circular external fixation and distraction osteogenesis in 13 dogs. *Vet Surg* 2014;43:316–329.
34. Webster CE, Marcellin-Little DJ, Koballa EM, et al. Evaluation of the geometric accuracy of computed tomography and microcomputed tomography of the articular surface of the distal portion of the radius of cats. *Am J Vet Res* 2019;80:976–984.
35. Fitzpatrick C, FitzPatrick D, Auger D, et al. A tibial-based coordinate system for three-dimensional data. *Knee* 2007;14:133–137.
36. Gulledge BM, Marcellin-Little DJ, Levine D, et al. Comparison of two stretching methods and optimization of stretching protocol for the piriformis muscle. *Med Eng Phys* 2014;36:212–218.
37. Su XY, Zhao JX, Zhao Z, et al. Three-dimensional analysis of the characteristics of the femoral canal isthmus: an anatomical study. *BioMed Res Int* 2015;2015:459612.
38. Su XY, Zhao Z, Zhao JX, et al. Three-dimensional analysis of the curvature of the femoral canal in 426 Chinese femurs. *BioMed Res Int* 2015;2015:318391.
39. Burdin V, Roux C, Lefevre C, et al. Modeling and analysis of 3-D elongated shapes with applications to long bone morphometry. *IEEE Trans Med Imaging* 1996;15:79–91.
40. Yang X, Lim Z, Jung H, et al. Estimation of instantaneous hand joint centers of rotation using 3D reconstructed hand skeleton motion from CT scans, in *Proceedings,* Hum Factor Ergon Soc Annu Meet 2018;681–685.
41. Kwon OY, Tuttle LJ, Commean PK, et al. Reliability and validity of measures of hammer toe deformity angle and tibial torsion. *Foot (Edinb)* 2009;19:149–155.
42. Carson MC, Harrington ME, Thompson N, et al. Kinematic analysis of a multi-segment foot model for research and clinical applications: a repeatability analysis. *J Biomech* 2001;34:1299–1307.
43. Clementz BG, Magnusson A. Assessment of tibial torsion employing fluoroscopy, computed tomography and the cryosectioning technique. *Acta Radiol* 1989;30:75–80.
44. Unis MD, Johnson AL, Griffon DJ, et al. Evaluation of intra- and interobserver variability and repeatability of tibial plateau angle measurements with digital radiography using a novel digital radiographic program. *Vet Surg* 2010;39:187–194.
45. Aghapour M, Bockstahler B, Kneissl S, et al. Femoral and tibial alignments in Chihuahuas with patellar luxation by radiograph: angular values and intra- and inter-observer agreement of measurements. *PLoS One* 2019;14:e0214579.
46. Homer LM, Gomes BAJ, Murphy MC, et al. Effect of osteoarthritis on the repeatability of patella tendon angle measurement in dogs. *Vet Surg* 2019;48:180–185.
47. Huang J, Tian F, Zhang Z, et al. Reliability and concurrent validity of angle measurements in lower limb: EOS 3D goniometer versus 2D manual goniometer. *J Orthop Translat* 2020;24:96–102.
48. Owen JL, Stephens D, Wright JG. Reliability of radiographic measurement of fracture angulation in children with femoral shaft fractures. *Can J Surg* 2007;50:115–118.
49. Barnes DM, Anderson AA, Frost C, et al. Repeatability and reproducibility of measurements of femoral and tibial alignment using computed tomography multiplanar reconstructions. *Vet Surg* 2015;44:85–93.
50. Meola SD, Wheeler JL, Rist CL. Validation of a technique to assess radial torsion in the presence of procurvatum and valgus deformity using computed tomography: a cadaveric study. *Vet Surg* 2008;37:525–529.
51. Miyake J, Murase T, Oka K, et al. Computer-assisted corrective osteotomy for malunited diaphyseal forearm fractures. *J Bone Joint Surg Am* 2012;94:e150.
52. Kai S, Sato T, Koga Y, et al. Automatic construction of an anatomical coordinate system for three-dimensional bone models of the lower extremities—pelvis, femur, and tibia. *J Biomech* 2014;47:1229–1233.